HHS Public Access

Author manuscript

Conf Proc IEEE Eng Med Biol Soc. Author manuscript; available in PMC 2020 March 23.

Published in final edited form as:

Conf Proc IEEE Eng Med Biol Soc. 2018 July ; 2018: 2366–2369. doi:10.1109/EMBC.2018.8512786.

A Mean Field Model of Acute Hepatic Encephalopathy

Jiangling Song[1,2], **Haoqi Sun**[2], **Jin Jing**[2,3], **Luis Carlos**[2], **Lingya Chao**[2], **Sydney S Cash**[2], **Rui Zhang**[1], **M.Brandon Westover**[2,*]

[1]The Medical Big Data Research Center of School Mathematics, Northwest University, China.

[2]Massachusetts General Hospital, Boston, MA.

[3]Nanyang Technological University, Singapore.

Abstract

Acute hepatic encephalopathy (AHE) is a common form of delirium, a state of confusion, impaired attention, and decreased arousal due to acute liver failure. However, the neurophysiological mechanisms underlying AHE are poorly understood. In order to develop hypotheses for mechanisms of AHE, our work builds on an existing neural mean field model for similar EEG patterns in cerebral anoxia, the bursting Liley model. The model proposes that generalized periodic discharges, similar to the triphasic waves (TPWs) seen in severe AHE, arise through three types of processes a) increased neuronal excitability; b) defective brain energy metabolism leading to impaired synaptic transmission; c) and enhanced postsynaptic inhibition mediated by increased GABA-ergic and glycinergic transmission. We relate the model parameters to human EEG data using a particle-filter based optimization method that matches the TPW inter-event-interval distribution of the model with that observed in patients EEGs. In this way our model relates microscopic mechanisms to EEG patterns. Our model represents a starting point for exploring the underlying mechanisms of brain dynamics in delirium.

I. INTRODUCTION

Acute hepatic encephalopathy (AHE) is a common condition, occurring in 30–45% of cirrhotic patients [2]. AHE is associated with decreased quality of life, increased hospitalization and increased mortality [7]. It is defined as a reversible clinical syndrome of impaired brain function occurring in patients with acute liver failure (ALF), and clinically it leads to impaired attention, confusion and decreased arousal[15]. Various abnormalities of the electroencephalogram (EEG), such as slower delta activity, periodic epileptiform discharges and triphasic-wave patterns (TPWs), are observed in AHE patients, which predict poor prognosis [1].

Neural computational modeling is widely used to shed light on the mechanisms underlying EEG patterns in both healthy and pathological states, including epilepsy, sleep disorders, and other neurological conditions. These models can be categorized according to the level of the target biological organization. Neural population models, first introduced by Beurle et. al.[4]

*The email of corresponding author: mwestover@mgh.harvard.edu.

in the 1950s, and later modified by Wilson and Cowan (1972)[16] and Da Silva et al. (1974) [11], simulate the activity of populations of neurons at a mesoscopic level. Population models have become an increasing popular method to study the relationship between EEG and neurophysiological mechanisms due to their ability to capture important brain dynamics in a simple yet biologically plausible way.

AHE is thought to result from accumulation in the brain of toxic substances from the gut that are normally metabolized and excreted by the liver, particularly ammonia[15], though the exact mechanisms underlying AHE remain elusive. It has been proposed that increased neuronal excitability, impaireds synaptic transmission secondary to impaired cellular bioenergetics, and postsynaptic inhibition, could be involved in the pathogenesis of AHE.

Elevated neuronal excitability is thought to occur secondary to hyperactivation of glutamate N-methyl-D-aspartate (NMDA) receptors. Ammonia levels are significantly increased in AHE patients [14], and elevated ammonia levels have been shown in ALF animal models to lead to over-activation of NMDA glutamate receptors, excessive formation of nitric oxide and cGMP, and ultimately increased neuronal excitability[12].Further, decreased expression of astrocytic glutamate transporters (EAAT-2)[9] and astrocytic glycine transporters (GLYT-1) [18] and concomitant increased levels of synaptic glutamate and glycine, agonist and co-agonist of NMDA receptors, respectively, are observed in ALF rat models and AHE patients, favoring NMDA-mediated excitatory neurotransmission and neuronal excitability.

Impaired synaptic transmission is another probable mechanism underlying AHE. Synaptic transmission is a metabolically active process which contributes immensely to the energy consumption by nervous tissue. It accounts for 30% of the brains adenosine triphosphate (ATP) usage [3]. In animal models of AHE, brain concentrations of ATP are significantly reduced, and this coincides with the onset of AHE-associated behavioral impairment and EEG changes [10].

A growing body of evidence suggests that enhanced gamma-aminobutyric acid (GABA)- and glycine-mediated postsynaptic inhibition may also be involved in the pathophysiology of AHE. Levels of pregnenolone-derived neurosteroids (e.g. allopregnanolone), potent selective positive allosteric modulators of the $GABA_A$ receptor, are significantly increased in experimental ALF models and in brains of hepatic coma patients [6].

Here, we aim to elucidate the mechanisms underlying AHE by evaluating whether the bursting Liley model[5], modified to include the aforementioned candidate mechanisms underlying AHE (increased excitability, impaired synaptic transmission, and enhanced postsynaptic inhibition), is able to quantitatively reproduce the pattern of TPWs observed in the EEGs of AHE patients. In our work, it means if some features of TPWs could be reproduced by the proposed model. We only consider periodicity, which is the key feature of TPWs and characterized by inter-event-interval (IEI) in this paper. While it is clear from this prior work that the model is able to produce GPD-like patterns, here we explore which parameter settings are able to quantitatively match key characteristics of real EEGs from patients with AHE.

II. NEURAL COMPUTATIONAL MODEL OF AHE

Our mean field model comprises excitatory and inhibitory neural populations, local synaptic connections, and thalamic input (Fig. 1). In mathematical terms the model is detailed as follows,

$$\begin{aligned}
&\tau_k \dot{V}_k(t) = V_k^{rest} - V_k(t) + \sum_l \psi_{lk}(V_k(t)) I_{lk}(t), \\
&\psi_{lk}(V_k(t)) = \frac{\left[V_{lk}^{eq} - V_k(t)\right]}{\left|V_{lk}^{eq} - V_k^r\right|}, \\
&\ddot{I}_{lk}(t) = -2\gamma_k \dot{I}_{lk}(t) - \gamma_k^2 I_{lk}(t) + e\gamma_k \Gamma_k(N_{lk} S_k(V_k(t) + p_{lk}(t)), \\
&S_k(V_k(t)) = Q_k^{max} / \left(1 + e^{-\sqrt{2}(V_k - \mu_k)/\sigma_k}\right).
\end{aligned} \tag{1}$$

where $l, k = e, i$, represent excitatory and inhibitory populations respectively. The interpretation and physiological ranges for the parameters of (1) are described in [5].

To model the effect of increased neuronal excitability, we increase the resting value of the maximum excitatory postsynaptic potential (EPSP) amplitude (corresponding to the model parameter Γ_e^{rest}) after calculating the equilibrium voltage of the EPSP, through multiplying by an amplification factor,

$$\Gamma_e^{rest} = \Gamma_e^{equ} * (1 + F_{am}), \tag{2}$$

where F_{am} is the amplification factor, Γ_e^{equ} is the equilibrium voltage of the EPSP.

To model increased GABAergic neurotransmission, we prolong the duration of the inhibitory postsynaptic potential (IPSP) by altering the decay rate constant γ_i, without changing its rise rate and peak amplitude. According to Bojak and Liley's work[5], the decay rate can be characterized through introducing

$$\gamma_i = \gamma_i^0 / \lambda_i, \tilde{\gamma}_i = \rho_i \gamma_i, \lambda_i = e^{\epsilon_i} - 1/\epsilon_i, \rho_i = e^{\epsilon_i}, \tag{3}$$

where γ_i^0 is the baseline synaptic time constant, ϵ_i is the control parameter relating to the decay time of the IPSP. Thus we increase ϵ_i and find the appropriate range of values that achieve the modeling goal.

To model the effect of impaired synaptic transmission, we model the postsynaptic potential amplitude (γ_k) as a variable with its own slow dynamics coupled to the presynaptic firing rate ($S_k(\cdot)$) and recovery time (τ_k^{rec}) according to the work of Ruijter et.al.[13],

$$\Gamma_k(t) = \left(\Gamma_k^{rest} - \Gamma_k(t)\right)/(\tau_k^{rec}) - p_k^{dep} S_k(h_k(t)) \Gamma_k(t), \tag{4}$$

where $k = e, i$, p_k^{dep} is the depletion constant because of the impaired synaptic transmission.

III. PARTICLE-FILTER-BASED PARAMETER ESTIMATION METHOD

Particle filtering (PF) is a technique for recursive Bayesian estimation. It employs mutation-selection sampling approaches to represent the posterior distribution of a stochastic process given noisy or partial observations. The general process of PF is based on the state transition function f and the measurement function h,

$$x_k = f(x_{k-1}, \theta_k, v_k), y_k = h(x_k, w_k),$$

where x is the state variable, $\boldsymbol{\theta}$ is the parameter vector, y is the measurement variable, w, v are noise variables, and k is the time step. For our model, $x = \{V_e, V_i, I_{ee}, I_{ei}, I_{ie}, I_{ii}, \Gamma_e, \Gamma_i\}$, y is the measured EEG signal, $h(x_k, w_k) = Cx_k + w_k$, $C = (-1, 0, \ldots, 0)_{1\times 18}$.

Our PF-based parameter estimation method can be described as follows:

- Step 1. Parameter $\boldsymbol{\theta}$ is sampled from initial distribution $\boldsymbol{\theta} \sim p(x, \boldsymbol{\theta}|y)$ to generate N particles $\{T_1, \ldots, T_N\}$. Here, the initial distribution is assumed to be a uniform distribution.
- Step 2. For each particle i, time-series data (model output) X_i is produced according to $f(x, \boldsymbol{\theta}_{k-1}, v)$.
- Step 3. The features F are calculated for X_i and y respectively. In our work, F is the inter-event-interval, which is applied to characterize the frequency and periodicity of signals.
- Step 4. Assuming w is normally distributed, then for each particle the likelihood of the measured signal can be expressed as

$$p_i = 1/\left(\sqrt{2\pi}\sigma_i\right)e^{-\frac{1}{2}\left(\frac{F_y - F_x}{\sigma_i}\right)^2},$$

  which is used to compare generated vs measured data, and $\frac{p_i}{N}$ is taken as the weight of each particle.
- Step 5. The log-likelihood of all particles in the k-th step is estimated by

$$P_k = log\left(\sum_{i=1}^{N} p_i/N\right) = log\left(\sum_{i=1}^{N} p_i\right) - logN\,.$$

- Step 6. To estimate the high likelihood values of the model parameters, high likelihood particles are increased and low ones are decreased. The inverse CDF method is used to re-sample particles[17]. Denoting $\{T_{k1}, \ldots, T_{kN}\}$, this selection results in the k-th step.
- Step 7. Repeat: Go back to step 2 until $|P_k - P_{k-1}| < \epsilon$.

IV. EXPERIMENTS AND RESULTS

A. Data

In this study, we analyze the scalp EEG from 5 AHE patients who were hospitalized at the Massachusetts General Hospital. Each epoch lasts for 30 min, on bipolar montage, and was re-sampled to 128Hz. Digital filters (0.5Hz high-pass and 60Hz notch filters) were applied to de-noise the data before further analysis.

B. Experiments and results

Model output analysis: In order to analyze the effect of AHE mechanisms included in previous on model behavior, we only change parameters $\{\tau_e^{rec}, \tau_i^{rec}, F_{am}, \gamma_i\}$ in equations (1) (2) and (3); other parameters are set to be their standard values (adapted from Ruijter et al., 2017). The Euler-Maruyama method is applied to solve the set of equations (1)–(4) and produce simulated EEG signals.

Fig. 2 shows the model output, representing 40s of simulated EEG sampled at 128 Hz with different values for τ_e^{rec} ($\tau_i = 1000$, $F_{am} = 0.8$, $\gamma_i = 0.0332$); these signals are bandpass filtered (following conventions for displaying clinical EEG data). We see that the larger τ_e^{rec}, the larger the inter-event-interval. This is also reflected in the mean values of IEI histogram. Table I gives the mean IEI values of model output under different parameter settings (τ_e^{rec}, τ_i, F_{am}, γ_i) We see that the larger τ_i^{rec} (or γ_i), the smaller the IEI. However, the similar values are obtained for different F_{am}, which may suggest that the relatively insignificant effect of F_{am} on IEI. For these reasons, in the following section, we only consider τ_e^{rec}, τ_i^{rec} as the estimated parameters.

Real data analysis: We used Neurobroswer [8] to annotate TPWs for each patient; this retrospective analysis of EEG data was carried out under an IRB approved protocol. The inter-event-interval (IEI) is defined as the interval between peaks of consecutive TPW. From these IEIs, we obtain the IEI histogram is obtained. Fig. 3 shows 10s EEG segments and corresponding IEI histograms for patient 1.

Parameter estimation: We first perform the PF-based parameter estimation method on simulated data, produced by the proposed model and a set of known parameters. The 20s simulated data (2056 samples) was generated with parameters $\{\tau_e^{rec} = 30,000, \tau_i^{rec} = 1000, F_{am} = 0.8, \gamma_i = 0.1\}$. The process of estimation is shown in Fig. 4. The red line represents simulated data ("Target"), and the green line is the model output of each estimation step. The last subplot shows the final result, and the corresponding estimated parameters $\{\hat{\tau}_e^{rec} = 30492.9616, \hat{\tau}_i^{rec} = 805.3513\}$. We see that the simulated waveform is similar close to that of the target according to IEI distribution. These results demonstrate the ability of the PF estimation approach for our model estimation task.

Next, we applied the PF-based parameter estimation method to real EEG data. The recorded EEG signals with TPWs are divided into 60s segments. Then the PF-based estimation

method is applied to approximate the parameters of EEG segments of randomly selected 60s EEG segments. Fig. 5 and 6 show the estimation results and corresponding IEI distribution (histograms) of patients 1 and 2. From Fig. 5, We see that the IEI histogram of real EEG data with AHE can be approximately reproduced by the proposed model with the estimated parameters $\tau_e^{rec} = 17434.1948$, $\tau_i^{rec} = 1098.3883$. Similar results can be obtained in patient 2 (Fig. 6). Fig. 7 depicts the IEI boxplots of estimation results for patients 1–5. The t-test results (H and p) suggest that there is no significant difference between corresponding IEI distributions. Thus, the proposed model is able to reproduce IEI histograms of AHE patients through tuning model parameters, where reproducing means aligning the statistical distribution of features extracted from model output and real EEG data.

V. CONCLUSION

This work explores three candidate mechanisms of triphasic waves (TPW) in the EEG of patients with severe AHE: 1) increased neuronal excitability; 2) impaired synaptic transmission; 3) increased GABA-ergic tone. Our work builds on an existing neural mean field model (NMFM) for similar EEG patterns in cerebral anoxia (the bursting Liley model). EEG signals from patients with TPW patterns are correlated with model output signals (simulated data) through characterizing one kind of feature: the inter-event-interval histogram. Matching of model output with the TPW EEG data is accomplished using particle-filter based optimization. This method is able to successfully reproduce key quantitative features (inter-event-interval histogram) of EEG data from actual patients with TPWs.

REFERENCES

[1]. Agrawal S, Umapathy S, and Dhiman RK, “Minimal hepatic encephalopathy impairs quality of life,” Journal of clinical and experimental hepatology, vol. 5, pp. S42–S48, 2015. [PubMed: 26041957]

[2]. Amodio P, Del Piccolo F, Pettenò E, Mapelli D, Angeli P, Iemmolo R, Muraca M, Musto C, Gerunda G, Rizzo C et al., “Prevalence and prognostic value of quantified electroencephalogram (eeg) alterations in cirrhotic patients,” Journal of hepatology, vol. 35, no. 1, pp. 37–45, 2001. [PubMed: 11495040]

[3]. Back T, Nedergaard M, and Ginsberg M, “The ischemic penumbra: pathophysiology and relevance of spreading depression-like phenomena,” Cerebrovascular Disease: Pathophysiology, Diagnosis and Management. Malden, Mass: Blackwell Science, pp. 276–286, 1998.

[4]. Beurle RL, “Poperties of a mass of cells capable of regenerating pulses,” Trans. Roy. Soc. (Lond) B, vol. 240, pp. 55–94, 1956.

[5]. Bojak I and Liley D, “Modeling the effects of anesthesia on the electroencephalogram,” Physical Review E, vol. 71, no. 4, p. 041902, 2005.

[6]. Butterworth RF, “Neurosteroids in hepatic encephalopathy: novel insights and new therapeutic opportunities,” The Journal of steroid biochemistry and molecular biology, vol. 160, pp. 94–97, 2016. [PubMed: 26589093]

[7]. D’amico G, Morabito A, Pagliaro L, Marubini E et al., “Survival and prognostic indicators in compensated and decompensated cirrhosis,” Digestive diseases and sciences, vol. 31, no. 5, pp. 468–475, 1986. [PubMed: 3009109]

[8]. Jing J, Dauwels J, Rakthanmanon T, Keogh E, Cash S, and Westover M, “Rapid annotation of interictal epileptiform discharges via template matching under dynamic time warping,” Journal of neuroscience methods, vol. 274, pp. 179–190, 2016. [PubMed: 26944098]

[9]. Knecht K, Michalak A, Rose C, Rothstein JD, and Butterworth RF, “Decreased glutamate transporter (glt-1) expression in frontal cortex of rats with acute liver failure,” Neuroscience letters, vol. 229, no. 3, pp. 201–203, 1997. [PubMed: 9237493]

[10]. Kosenko E, Kaminsky Y, Grau E, Miñana M-D, Marcaida G, Grisolía S, and Felipo V, “Brain atp depletion induced by acute ammonia intoxication in rats is mediated by activation of the nmda receptor and na+, k+-atpase,” Journal of neurochemistry, vol. 63, no. 6, pp. 2172–2178, 1994. [PubMed: 7964737]

[11]. Lopes da Silva F, Hoeks A, Smits H, and Zetterberg L, “Model of brain rhythmic activity,” Biological Cybernetics, vol. 15, no. 1, pp. 27–37, 1974.

[12]. Marcaida G, Felipo V, Hermenegildo C, Miñana M-D, and Grisolia S, “Acute ammonia toxicity is mediated by the nmda type of glutamate receptors,” FEBS letters, vol. 296, no. 1, pp. 67–68, 1992. [PubMed: 1346118]

[13]. Ruijter BJ, Hofmeijer J, Meijer HGE, and van Putten MJAM, “Synaptic damage underlies eeg abnormalities in postanoxic encephalopathy: A computational study,” Clinical neurophysiology, vol. 128, no. 9, pp. 1682–1695, 2017. [PubMed: 28753456]

[14]. Weiss N, Saint Hilaire PB, Colsch B, Isnard F, Attala S, Schaefer A, del Mar Amador M, Rudler M, Lamari F, Sedel F et al., “Cerebrospinal fluid metabolomics highlights dysregulation of energy metabolism in overt hepatic encephalopathy,” Journal of hepatology, vol. 65, no. 6, pp. 1120–1130, 2016. [PubMed: 27520878]

[15]. Wijdicks EF, “Hepatic encephalopathy,” New England Journal of Medicine, vol. 375, no. 17, pp. 1660–1670, 2016. [PubMed: 27783916]

[16]. Wilson HR and Cowan JD, “Excitatory and inhibitory interactions in localized populations of model neurons,” Biophysical journal, vol. 12, no. 1, pp. 1–24, 1972. [PubMed: 4332108]

[17]. Zio EPG, “Particle filtering prognostic estimation of the remaining useful life of nonlinear components,” Clinical neurophysiology, vol. 96, no. 3, pp. 403–409, 2011.

[18]. Zwingmann C, Desjardins P, Hazell A, Chatauret N, Michalak A, and Butterworth RF, “Reduced expression of astrocytic glycine transporter (glyt-1) in acute liver failure,” Metabolic brain disease, vol. 17, no. 4, pp. 263–273, 2002. [PubMed: 12602503]

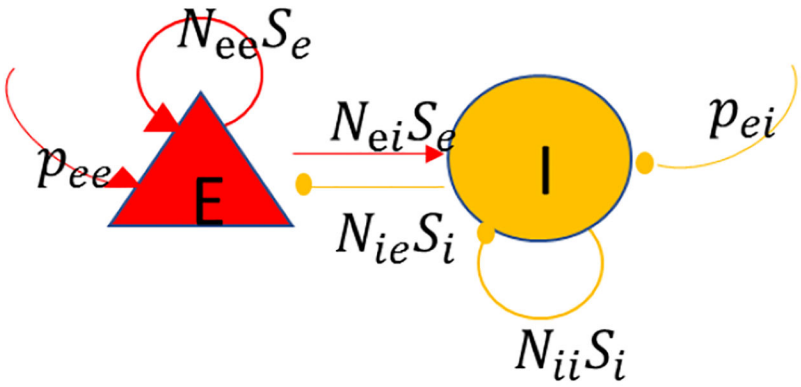

Fig. 1.

Sketch of Liley model. Two distinct macrocolumns with excitatory (E) and inhibitory (I) neural populations are shown, as well as their local synaptic connections (N_{jk}), and mean firing rate S_k.

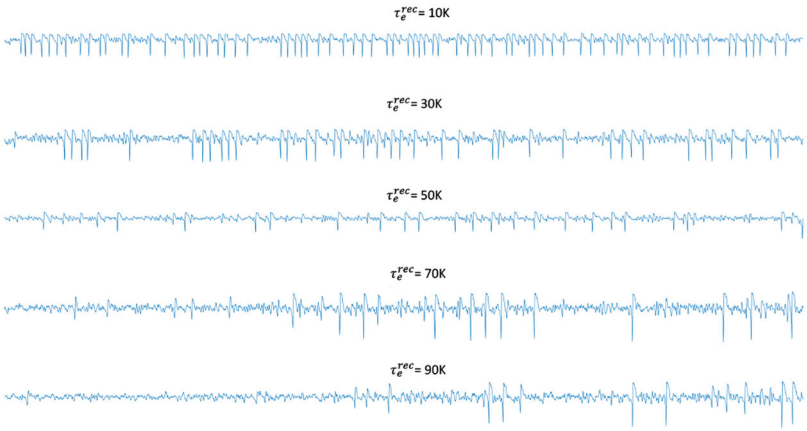

Fig. 2.

Model output, showing 40s of simulated EEG sampled at 128 Hz with different values of τ_e^{rec} (10K:20K:90K).

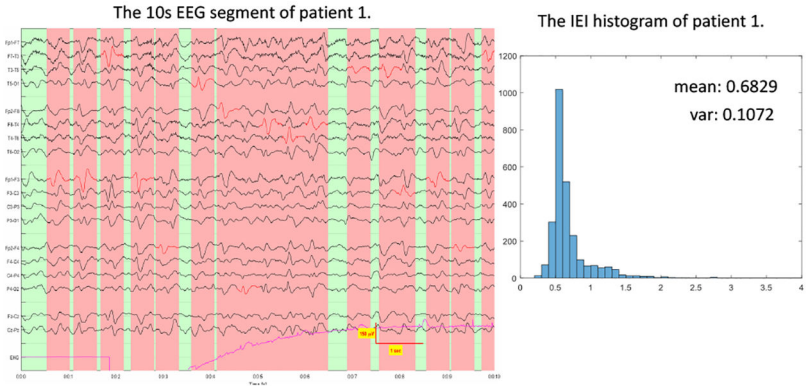

Fig. 3.

10s of clinical EEG data from patient 1 and its corresponding inter-event-interval historgram.

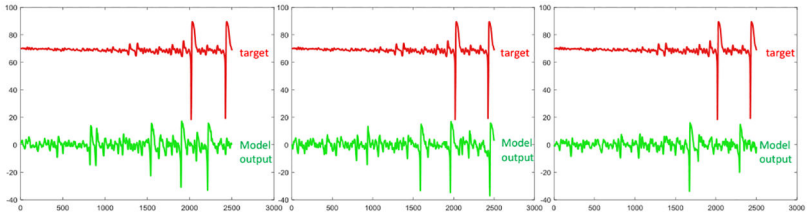

Fig. 4.

The iteration results of parameter (τ_e^{rec}, τ_i^{rec}) estimation on simulated data (20s).

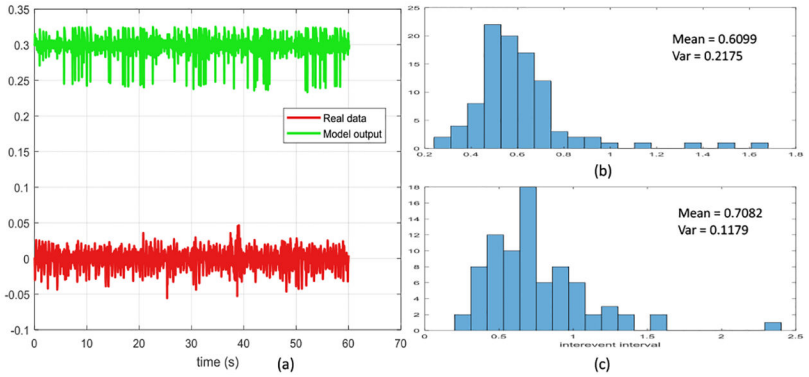

Fig. 5.

Patient 1: (a) EEG data from a patient with TPWs and simulated signal using estimated parameters;(b) IEI histogram of model output; (c) IEI histogram of real data.

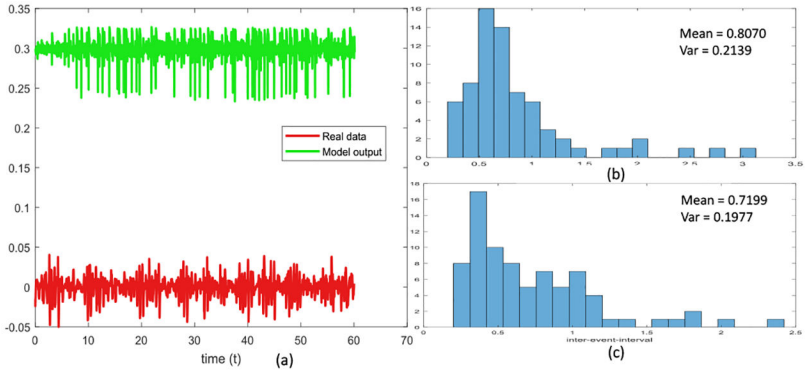

Fig. 6.

Patient 2: (a) EEG data from a patient with TPWs and simulated signal using estimated parameters;(b) IEI histogram of model output; (c) IEI histogram of real data.

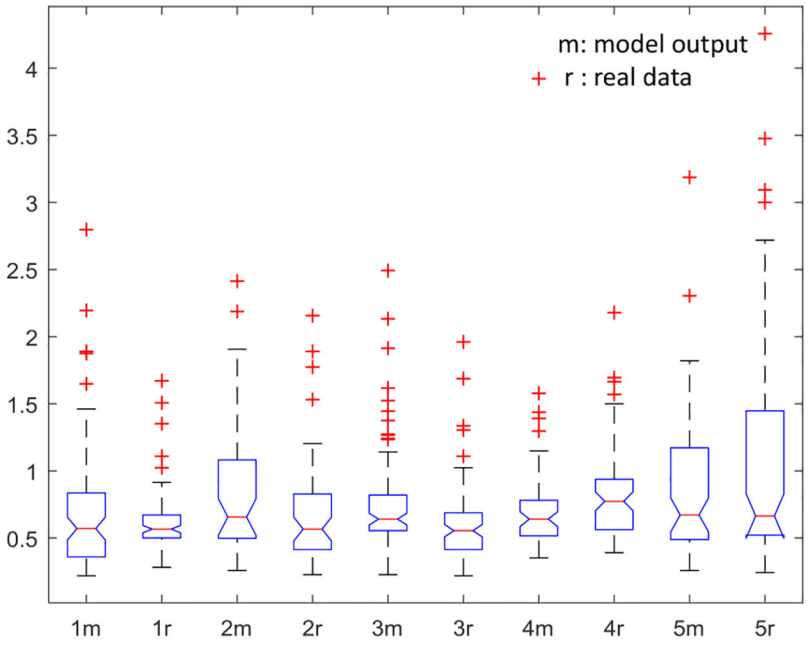

Fig. 7.

The IEI box-plots of model output and real data for patients 1–5, no.(m/r) means the model output/real data for patient no..

TABLE I

Mean IEI values of model output under different parameter settings (τ_e^{rec}, τ_i, F_{am}, γ_i)

F_{am}	τ_e^{rec}	τ_i^{rec}	γ_i
0.6941(0.1)	0.5377 (10K)	0.8709(100)	1.2525 (0.0051)
0.6982(0.3)	0.7024(30K)	8085(300)	1.1709 (0.0054)
0.6241(0.5)	0.8515(50K)	0.7783(500)	1.2831 (0.0061)
0.6290(0.7)	1.045(70K)	0.7792(700)	1.0766 (0.0091)
0.6522(0.9)	1.012(90K)	0.7314(900)	0.6183(0.0332)